Flow through percolation clusters: NMR velocity mapping and numerical simulation study

Andreas Klemm, Rainer Kimmich, and Markus Weber
Sektion Kernresonanzspektroskopie, Universität Ulm, 89069 Ulm, Germany
(Received 18 July 2000; published 29 March 2001)

Three- and (quasi-)two-dimensional percolation objects have been fabricated based on Monte Carlo generated templates. The object size was up to 12 cm (300 lattice sites) in each dimension. Random site, semicontinuous swiss-cheese, and semicontinuous inverse swiss-cheese percolation models above the percolation threshold were considered. The water-filled pore space was investigated by nuclear magnetic resonance (NMR) imaging and, after exerting a pressure gradient, by NMR velocity mapping. The spatial resolutions of the fabrication process and the NMR experiments were 400 μm and better than 300 μm, respectively. The experimental velocity resolution was 60 μm/s. The fractal dimension, the correlation length, and the percolation probability can be evaluated both from the computer generated templates and the corresponding NMR spin density maps. Based on velocity maps, the percolation backbones were determined. The fractal dimension of the backbones turned out to be smaller than that of the complete cluster. As a further relation of interest, the volume-averaged velocity was calculated as a function of the probe volume radius. In a certain scaling window, the resulting dependence can be represented by a power law, the exponent of which was not yet considered in the theoretical literature. The experimental results favorably compare to computer simulations based on the finite-element method (FEM) or the finite-volume method (FVM). This demonstrates that NMR microimaging as well as FEM/FVM simulations reliably reflect transport features in percolation clusters.

DOI: 10.1103/PhysRevE.63.041514 PACS number(s): 61.43.Hv, 47.55.Mh, 47.53.+n

I. INTRODUCTION

The objective of this study is to explore laws governing flow in two- and three-dimensional objects modeling porous media. The description by characteristic parameters is of particular interest as demonstrated by the numerous papers in literature dealing with such problems (see, for instance, Refs. [1–5]). The present investigations refer to Monte Carlo generated percolation clusters as well as to real model objects that have been fabricated on the basis of the Monte Carlo generated templates. Numerical simulations based on the finite-element method (FEM) or the finite-volume method (FVM) on the one hand are compared with experimental results of nuclear magnetic resonance (NMR) microscopy techniques on the other.

Three different, well-defined percolation models [4,6,7] have been considered. (a) *Random site percolation*: Sites on a square or cubic lattice are occupied with a probability p in the vicinity of the percolation threshold that is characterized by the critical occupation probability p_c. Neighboring occupied sites are connected by pores with a cross section corresponding to the lattice constant a or integer multiples of it. The total subsets of connected lattice sites are called clusters. For $p>p_c$, sample-spanning clusters occur that can be examined with respect to transport properties. Adler *et al.* suggested the use of this model to describe Fontainebleau sandstone [9]. (b) *''Swiss cheese'' percolation* [8]: Circular or spherical obstacles of a certain radius are randomly distributed in a semicontinuous transport medium irrespective of any overlap. The pore space is then formed by the interstitial space. (c) *''Inverse swiss-cheese'' percolation*: Circular or spherical voids are placed at random in a semicontinuous matrix irrespective of any overlap. The pore space consists of the entity of the (partially overlapping) voids.

In the latter two cases, ''semicontinuous'' means that the obstacle or void positions coincide with grid points of a certain discrete square or cubic base lattice (e.g., of size $64\times64\times64$ in one of the systems to be considered here). In the present case, the respective radius of the obstacles and voids was chosen to be $2a$, where a is the base lattice constant [12]. That is, the obstacles or voids are allowed to ''continuously'' overlap each other. Note however, that the actual ''circular'' or ''spherical'' shape of the obstacles and voids can only be approximated by a point-symmetric distribution of discrete pixels or voxels, of course.

In order to put the results concerning flow through the percolation cluster on a reliable and mutually consistent basis, we have studied clusters characterized by the same parameters both in real NMR microscopy experiments and in FEM/FVM simulations. That is, clusters (in the three-dimensional case chosen without any unsuspended ''islands'' that cannot be realized in the model objects to be fabricated) were first defined using a random number generator. These data sets were then used as matrix patterns for the FEM/FVM simulations and as templates for the fabrication of real model objects. The real model objects were then filled with water pressed through the percolation cluster. Clearly, only the ''infinite'' cluster can be reached in this way, whereas any isolated ''finite'' clusters remain inaccessible to NMR experiments. Spin density and velocity maps of the water in the pores were recorded with the aid of four- or six-dimensional space- and velocity-encoding sequences of radio frequency and field gradient pulses [13] in the case of (quasi-)two- or three-dimensional percolation clusters, respectively.

II. EXPERIMENTAL AND NUMERICAL METHODS

Figure 1 shows the radio frequency and field gradient pulse scheme [13] used for the spin density and velocity

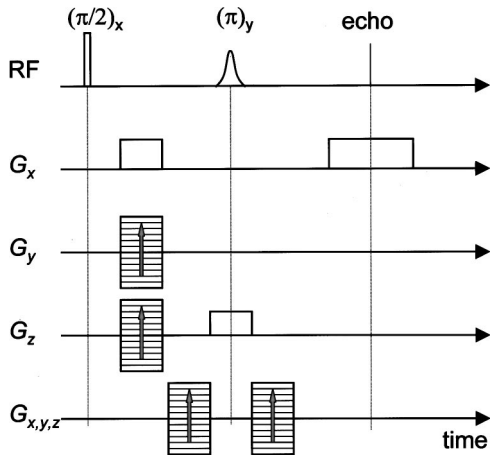

FIG. 1. Radio frequency and field gradient pulse sequence used for the NMR velocity mapping experiments. A Hahn spin echo is generated by the ordinary $\pi/2$-π RF pulse sequence. The π pulse is applied in the presence of a G_z gradient in order to select the sample volume of interest and to suppress signals from the water supply hoses. The three spatial dimensions are probed by gradient pulses G_x (frequency encoding), and G_y and G_z (phase encoding). The latter two gradients are independently incremented in a series of successive transients. In order to acquire the velocity vector field, in principle, three more dimensions must be scanned. The velocity components are phase encoded by the three unipolar and ''area''-matched gradient pulse pairs flanking the π pulse. These gradient pulses are again incremented in successive transients, independently of each other and of the spatial encoding pulses. The data set acquired in this way consists of four- (two-dimensional objects) or six-dimensional (three-dimensional objects) matrices for the reciprocal spaces of the position and velocity vectors. Fourier transforms in all of these dimensions lead to a conjugated data set allocating a velocity vector to each voxel.

TABLE I. Comparison of the fractal dimensions of the pore spaces and their backbones evaluated from Monte Carlo and FEM-simulated percolation clusters and experimental data sets obtained with corresponding model objects. The data refer to averages for all mean porosities considered. The error limits are rms deviations in the corresponding data sets.

	Site percolation	Swiss cheese	Inverse swiss cheese
d_f^{MC}	1.86 ± 0.02	1.65 ± 0.03	1.81 ± 0.03
d_f^{exp}	1.83 ± 0.03	1.66 ± 0.04	1.83 ± 0.03
d_{fback}^{FEM}	1.50 ± 0.03	1.24 ± 0.06	1.5 ± 0.1
d_{fback}^{exp}	1.46 ± 0.03	1.41 ± 0.05	1.4 ± 0.1

mapping NMR experiments. A 4.7-T Bruker magnet with a 40-cm, horizontal room-temperature bore was employed. The radio frequency console was home made and controlled by a PC. The spatial resolution of the spin density or velocity maps was better than 300 μm in all spatial dimensions.

The percolation model objects were fabricated using a circuit board plotter (for details see Refs. [10–12]). Figure 2 shows a typical two-dimensional random site percolation cluster generated on a square lattice of 300×300 sites. The occupation probability relative to the percolation threshold is $p = p_c + 0.028$ (where $p_c = 0.5927$ for the Euclidean dimension $d_E = 2$ [14]). Based on the Monte-Carlo-generated template (graph on the left), a 12 cm $\times$ 12 cm model object was fabricated with a mechanical resolution of 400 μm (photograph in the middle). Eight identical, 2-mm-thick layers with a two-dimensional percolation network structure were stacked in order to guarantee a good signal-to-noise ratio in the experiments. The object was filled with water, and a spin density map was recorded with a digital resolution of 300 μm (picture on the right). Visual inspection already

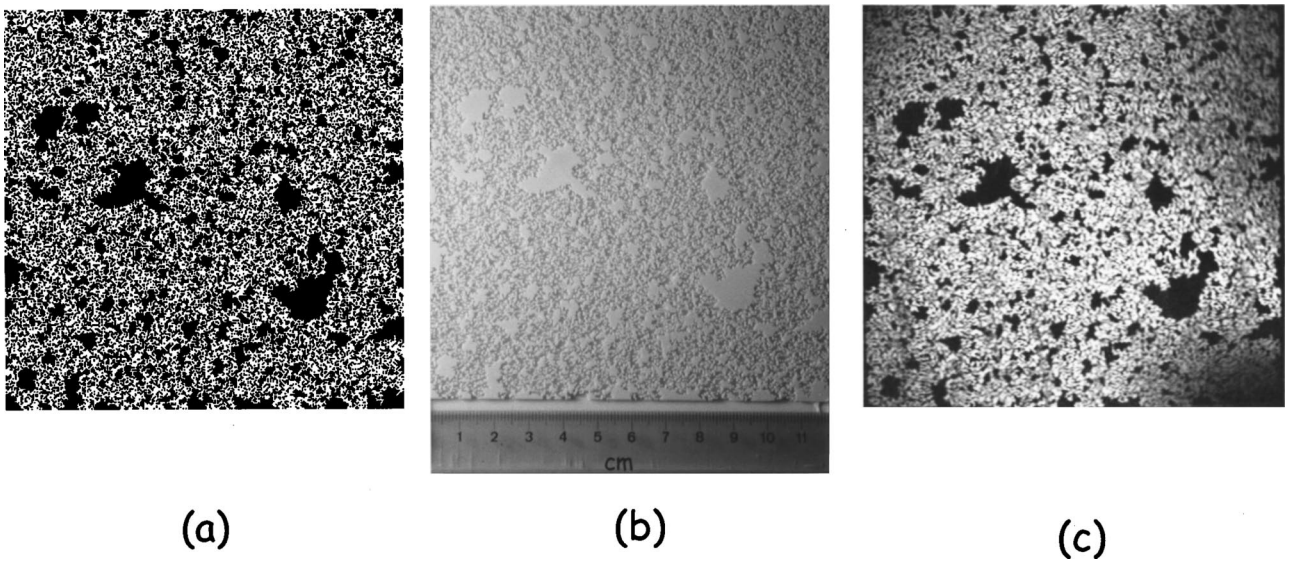

FIG. 2. Typical two-dimensional random site percolation object generated on a square lattice of 300×300 sites. The sites are occupied with a probability $p = p_c + 0.028$, where p_c is the percolation threshold. The fractal dimension is $d_f = 1.87$. (a) Graph of the Monte Carlo generated template. (b) Photograph of the 12 cm $\times$ 12 cm model object fabricated according to the Monte Carlo generated template. The mechanical resolution is 400 μm. (c) Spin density map of the water-filled pore space. The digital resolution was 290 μm (512×512). (A color-coded version of this figure can be retrieved via www.uni-ulm.de/nmr/)

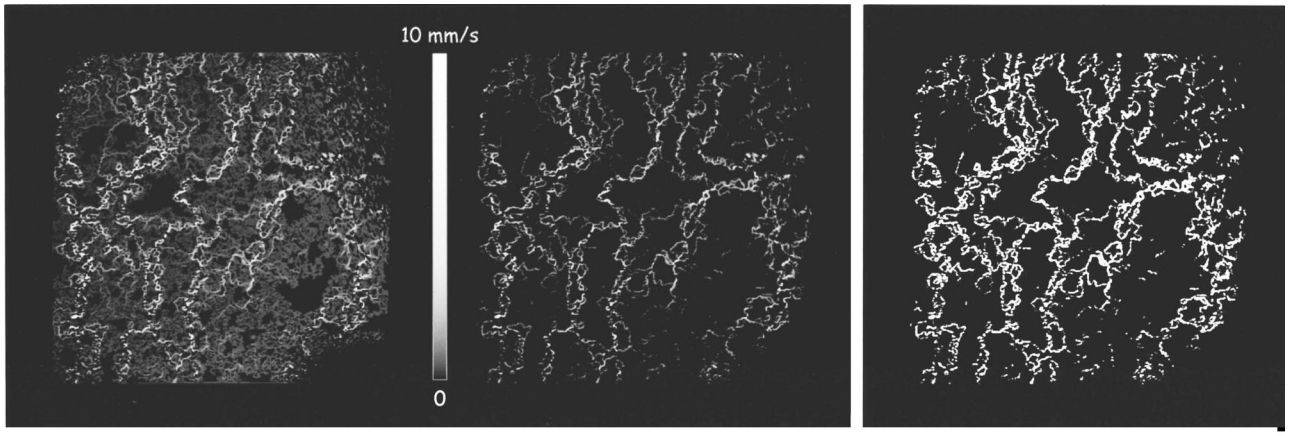

FIG. 3. Maps of the velocity magnitude $v=\sqrt{v_x^2+v_y^2}$ and backbone of the two-dimensional random site percolation model object shown in Fig. 2. The pore space was filled with water and a pressure gradient was exerted. The velocity maps were acquired using the pulse scheme shown in Fig. 1. (a) Velocity gray shade map as recorded. The ''black'' pixels of the corresponding black-and-white converted spin density map, that is, the pixels representing the matrix are screened off. The maximum velocity was $v_m=7.2$ mm/s. (b) Velocity gray shade map with all ''static'' pore space pixels (defined by $v\leqslant v_n$) blackened. The rms velocity noise level was $v_n=0.6$ mm/s. (c) Percolation backbone after black-and-white conversion of the velocity map (b) ($d_f=1.50$). (A color-coded version of this figure can be retrieved via www.uni-ulm.de/nmr/)

suggests that the fabrication process as well as the NMR imaging procedure reproduce all structural details with great fidelity.

The spin density maps for the whole clusters and for the backbones (subscript ''back'') can be black-and-white converted as described in Ref. [10]. In Table I the structural properties derived from the NMR experiments (subscript ''exp''), namely, the fractal dimensions of the percolation clusters, are compared with Monte Carlo (subscript ''MC'') and FEM simulation data. The black pixels are then considered to represent the solid matrix. This matrix pixel set was used as a mask to screen off the matrix in the velocity maps recorded with flowing water.

In the flow experiments, water was pumped through the objects using a pericyclic pump. The percolation backbone, which is the voxel subset of the pore space that contributes to transport across the sample [15], was determined with the aid of maps of the velocity magnitude for the (quasi-)two- or three-dimensional cases, $v=\sqrt{v_x^2+v_y^2}$ and $v=\sqrt{v_x^2+v_y^2+v_z^2}$, respectively. As a first step, all matrix voxels in the velocity maps were blackened using the matrix masks deduced from the black-and-white converted spin density maps. In this way, the contribution of noise from matrix voxels, whose phase distribution is falsely interpreted by the Fourier processing analysis as a velocity distribution, was avoided. Excluding the matrix voxels from Fourier processing prevents any velocity artifacts of this sort.

In the second step, the (true) velocity noise level in the pore space, v_n, was determined as the root-mean-square (rms) velocity in stagnant water. The average noise level was determined to be about 5% of the maximum velocity v_{max}. This value compares well with that found in a test experiment with Hagen/Poiseuille flow in a pipe. The velocity maps of the pore space were then treated in the following way. The pixel subset that has velocities $v\leqslant v_n$ was defined as a ''static'' pixel subset. Blackening all such static pore space pixels yields the backbone of the percolation cluster deprived from all dead ends [11]. Figures 3(c) and 4(b) show (quasi-)two- and three-dimensional examples, respectively.

FEM and FVM computer simulations of the velocity field in the pore space were carried out using the commercial software packages ANSYS/FLOTRAN 5.5 and FLUENT 5.3, respectively (compare Ref. [16]). In the case of large objects such as the 12 cm$\times$12 cm site percolation cluster displayed in Fig. 2, the FVM simulation variant was found to be superior. The convergence criterion was fixed to a residuum of $\epsilon=10^{-5}$. The matrix points were represented by 3×3 ''knots'' or ''elements.'' Obstacles in the pore space are defined by $v=0$ at the corresponding knots. In this way, periodic meshing was possible so that the same resolution applies to all flow paths. In the simulations all pertinent parameters of the NMR experiments were anticipated, that is, the fluid viscosity, the pressure difference exerted to the objects, and the object size. Figure 5 shows a comparison of experimental and simulated flow patterns in a random site percolation cluster.

III. RESULTS

In Fig. 6, a comparison of the three different percolation models mentioned above is represented. The Monte Carlo generated templates, on the basis of which (quasi-)two-dimensional model objects were fabricated, are shown in the first row (a). After filling the objects with water and exerting a stationary pressure gradient, the flow patterns through the clusters were recorded using the pulse scheme shown in Fig. 1. Blackening the velocity noise contrasts of all pixels that are known from the black-and-white converted spin density

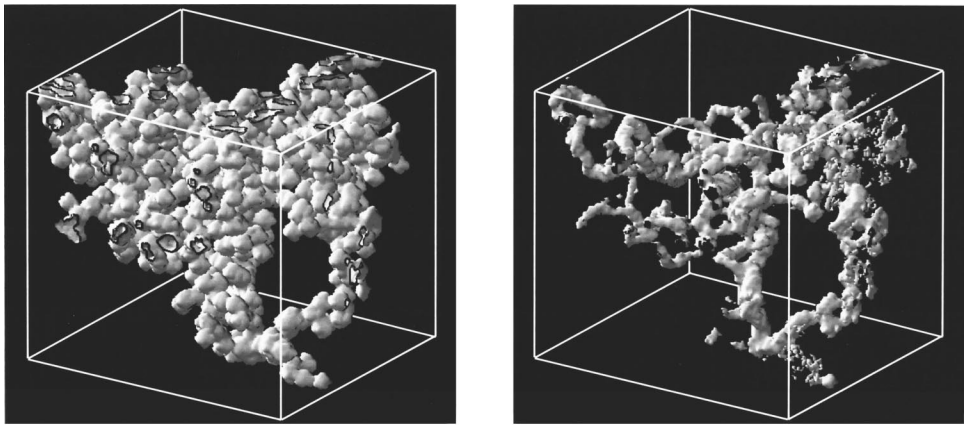

FIG. 4. Projections of three-dimensional spin density maps of an inverse swiss cheese model object filled with water. This object consists of one sample-spanning percolation cluster only. The data were recorded with the pulse scheme shown in Fig. 1. The object size is 3.2 cm×3.2 cm×3.2 cm. The size of the cubic lattice on which the cluster was generated is 64×64×64 sites. The mean porosity of the model object in which all isolated clusters were omitted is $p=0.087$. (The mean porosity of the total network including all isolated clusters would be 0.273.) (a) Complete percolation cluster as recorded in the form of a spin density map. The fractal dimension is $d_f=2.29$ (evaluated from the spin density map) or $d_f=2.292$ (determined from the Monte Carlo simulated template). (b) Percolation backbone derived on the basis of a velocity map recorded in the same object. The magnitude of the velocity $v=\sqrt{v_x^2+v_y^2+v_z^2}$ is represented in the range 0.85 mm/s$<v<$16.65 mm/s, that is, between the velocity noise level v_n in the pore space on the one hand, and the maximum value v_m on the other. The total flow rate was 59.3 mm^3 s^{-1}. The fractal dimension of the backbone was evaluated as $d_f=1.98$. (A color-coded version of this figure can be retrieved via www.uni-ulm.de/nmr/)

maps to belong to the solid matrix, led to the velocity maps shown in the third row (c). The second row (b) shows FEM simulations of these flow patterns. The fourth row (d) finally represents the percolation backbones obtained by blackening all pore space voxels in the velocity maps with velocities below the noise level.

The spin density and velocity maps were evaluated using the so-called sandbox method [10,11]. The quantities of interest are the volume-averaged porosity and the volume-averaged velocity. N_p probe circles (in the three-dimensional case, spheres) of varying radius r are first placed randomly at positions $\boldsymbol{r_k}$ within the map in such a way that the probe volumes are inside the sample and the center of the probe volume is in the pore space. Then the average values of the observables are formed for the N_V voxels at positions $\boldsymbol{r_j}$ inside the probe volume. Finally, the arithmetic mean of the data set for the N_p probe volumes with a given radius r is taken. In other words, the volume-averaged porosity is defined as

$$\overline{\rho}_V(r)=\frac{1}{N_p}\sum_{k=1}^{N_p}\frac{1}{N_V}\sum_{j=1}^{N_V}\rho(\boldsymbol{r_j}), \tag{1}$$

where $r\geqslant|\boldsymbol{r_k}-\boldsymbol{r_j}|$, and the density function

$$\rho(\boldsymbol{r_j})=\begin{cases}0 & \text{site } \boldsymbol{r_j} \text{ not occupied}\\ 1 & \text{site } \boldsymbol{r_j} \text{ occupied.}\end{cases} \tag{2}$$

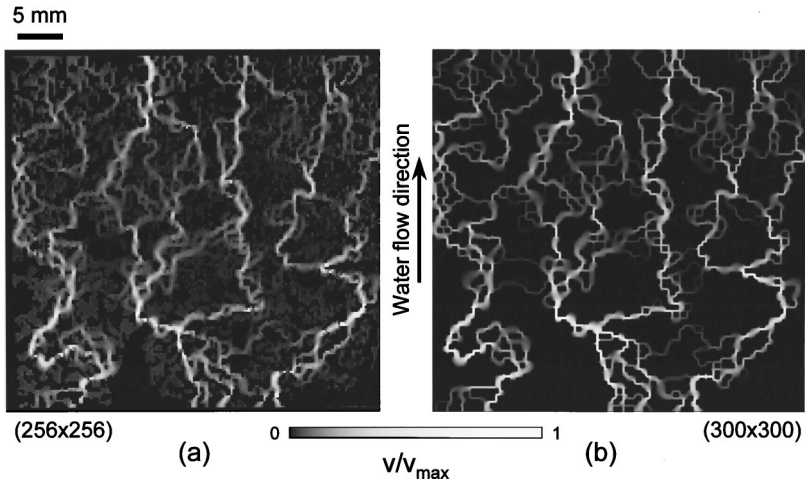

FIG. 5. Comparison of a NMR velocity map (a) and its FEM-simulated counterpart (b) of a two-dimensional random site percolation cluster on a 100×100 square lattice ($p=0.64$, $p-p_c=0.047$, $d_f=1.88$). The pixel resolutions are 256×256 and 300×300, respectively. (A color-coded version of this figure can be retrieved via www.uni-ulm.de/nmr/)

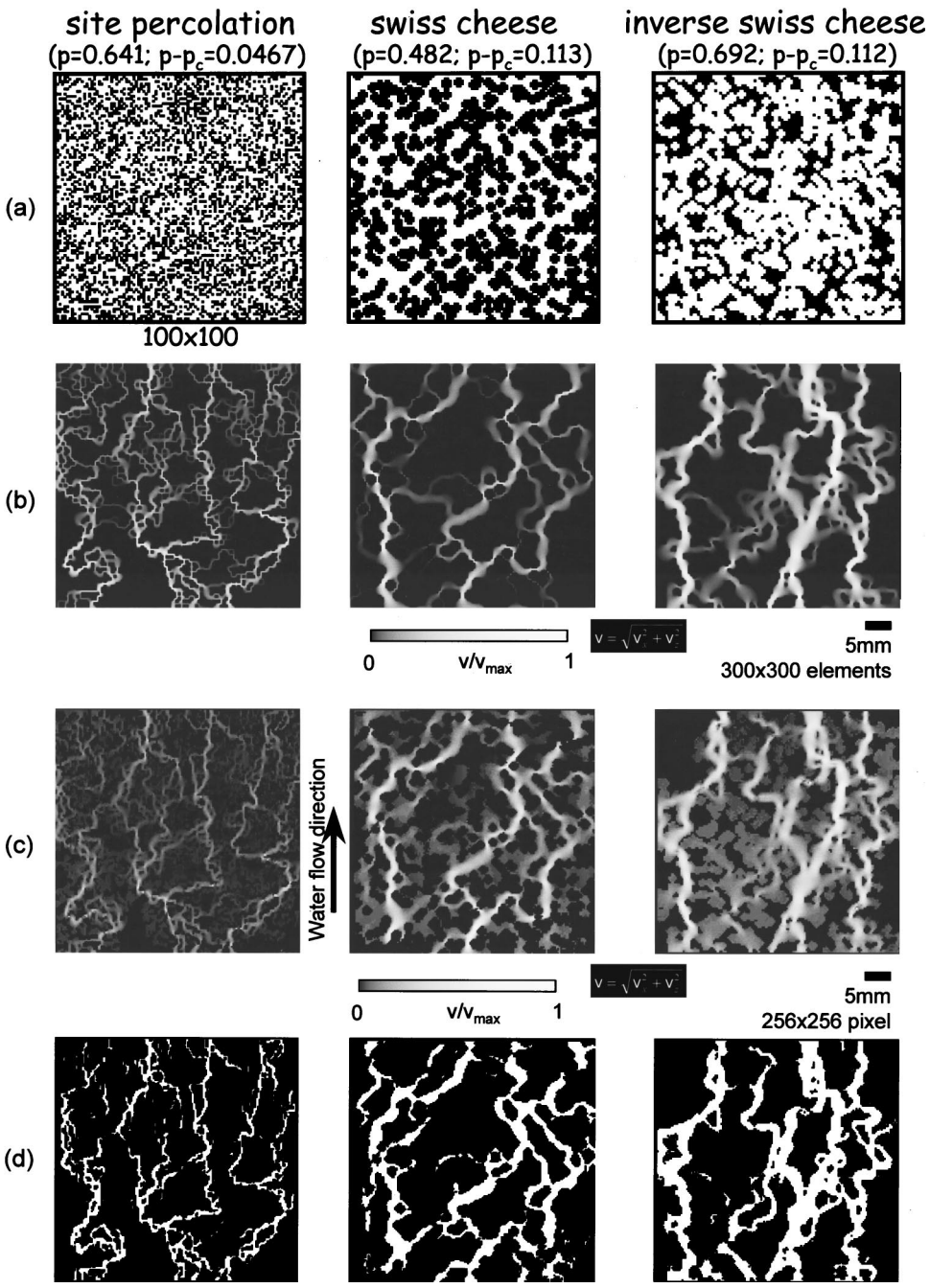

FIG. 6. Comparison of two-dimensional percolation models. (i) ''Site percolation,'' $p=0.641$, $p-p_c=0.0467$; (ii) ''swiss cheese,'' $p=0.482$, $p-p_c=0.113$; (iii) ''inverse swiss cheese,'' $p=0.692$, $p-p_c=0.112$. Row (a), Monte Carlo generated templates (pore space rendered in white). Row (b), FEM-simulated velocity maps. Row (c), experimental velocity maps recorded with the aid of the pulse scheme in Fig. 1 in water-filled model objects to which a pressure gradient is exerted. The maximum velocity magnitude is, depending on the individual experimental parameter setup, of the order of 10 mm/s. Row (d), backbones derived from the experimental velocity maps. Matrix pixels are blackened based on black-and-white converted spin density maps. (A color-coded version of this figure can be retrieved via www.uni-ulm.de/nmr/)

It can be evaluated from the black-and-white converted spin density maps [10]. The volume-averaged velocity has the analogous form

$$\overline{v}_V(r)=\frac{1}{N_p}\sum_{k=1}^{N_p}\frac{1}{N_V}\sum_{j=1}^{N_V}v(\boldsymbol{r}_j), \tag{3}$$

where again $r\geqslant|\boldsymbol{r}_k-\boldsymbol{r}_j|$. In this case, the evaluation directly refers to maps of the velocity magnitude in two or three dimensions, $v=\sqrt{v_x^2+v_y^2}$ and $v=\sqrt{v_x^2+v_y^2+v_z^2}$, respectively.

The volume-averaged porosity is characterized by three characteristic parameters [see Fig. 7(a)]: the fractal dimension d_f, the percolation probability P_∞, and the correlation length ξ. The fractal dimension is defined in the scaling window where the volume-averaged porosity obeys a power law of the form

$$\overline{\rho}_V(r)\propto r^{d_f-d_E}, \tag{4}$$

where d_E is the Euclidean dimension. This law applies to $r<\xi$. The correlation length ξ is defined as the mean distance of two occupied lattice points within the same finite cluster. Above the correlation length, i.e., for $r>\xi$ the volume-averaged porosity takes a constant plateau value corresponding to the percolation probability P_∞. This quantity is defined as the probability that a site belongs to the ''infinite'' cluster traversing the whole sample [17].

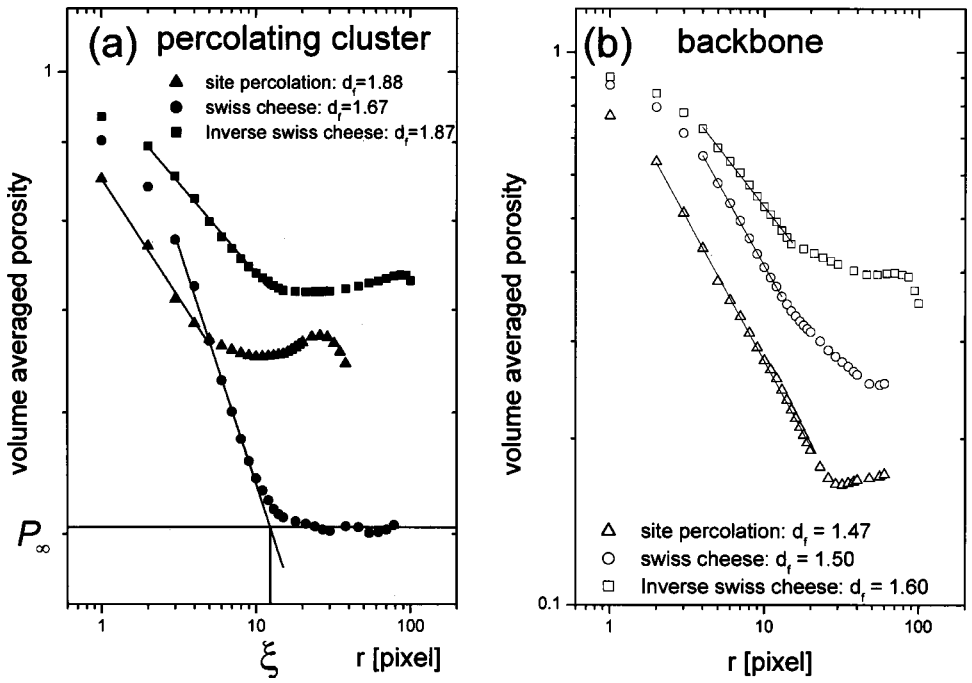

FIG. 7. Volume-averaged porosity of (a) the total percolation clusters and (b) the corresponding backbones as a function of the probe volume radius. The data have been evaluated from experimental spin density maps according to Eq. (1), and refer to the three percolation models characterized in Fig. 6 (''Site percolation,'' $p=0.641$, $p-p_c=0.0467$; ''swiss cheese,'' $p=0.482$, $p-p_c=0.113$; ''inverse swiss cheese,'' $p=0.692$, $p-p_c=0.112$). The solid lines represent the scaling behavior corresponding to Eq. (4). Deviations from the power law behavior at small probe volume radii are due to the fact that the pore dimensions vary in discrete steps so that starting from a certain probe volume center in the pore space, the first matrix pixel enters the averaging process in full only in a distance of a few pixels. The fluctuations of the data points above the correlation length are caused by the finite object size. The average then is restricted by the reduced number of probe volumes that can be placed within the sample.

Figure 7 shows plots of the volume-averaged porosity as a function of the probe volume radius. The evaluation was carried out on the basis of Eq. (1) from experimental spin density maps for the three percolation models. The characteristic parameters are given in the plots. The analysis of the Monte-Carlo-simulated templates [Fig. 2(a)] leads to equivalent results. This demonstrates that the experimental and data processing protocols lead to reliable results.

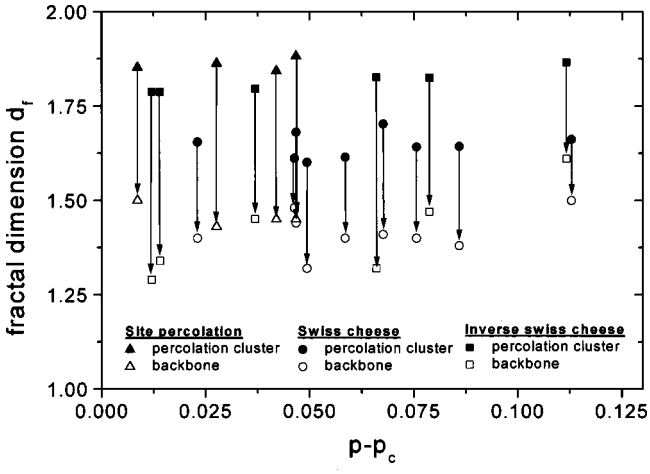

FIG. 8. Fractal dimensions of the total percolation clusters and their backbones as a function of $p-p_c$. The data refer to experimental NMR data and refer to the three percolation models characterized in Fig. 6 [''site percolation,'' ''swiss cheese,'' and ''inverse swiss cheese'' (see Figs. 6 and 7].

In Fig. 8, the fractal dimensions evaluated from the power law section of the volume-averaged porosity according to Eq. (4) is plotted as a function of the occupation probability for all three percolation models and their backbones are derived from experimental NMR data. It appears that the relation between the fractal dimensions of the backbone, d_{fback}^{exp}, and of the total percolation cluster, d_f^{exp}, averaged over all three models and all mean porosities investigated,

$$\langle d_{fback}^{exp}\rangle = \langle d_f^{exp}\rangle - (0.3 \pm 0.1), \tag{5}$$

is valid. The error limits represent the rms deviation in the data set considered. The average fractal dimension of all experimentally determined backbones was found to be $\langle d_{fback}^{exp}\rangle = 1.46$.

This value may be compared with Monte Carlo based simulation data for a site percolation cluster reported in the literature, see Refs. [18,19]. In these studies, the backbone was defined as the ensemble of all voxels that are connected with the surface by at least two pathways. Based on this definition, a value of $d_{fback}=1.64$ was evaluated [19]. On the other hand, the ''skeleton'' was defined consisting of the set of all shortest pathways to the surface [18]. The corresponding fractal dimension was reported to be $d_f^{sk}=1.10$. Note that in real flow, the preferential transport pathways are

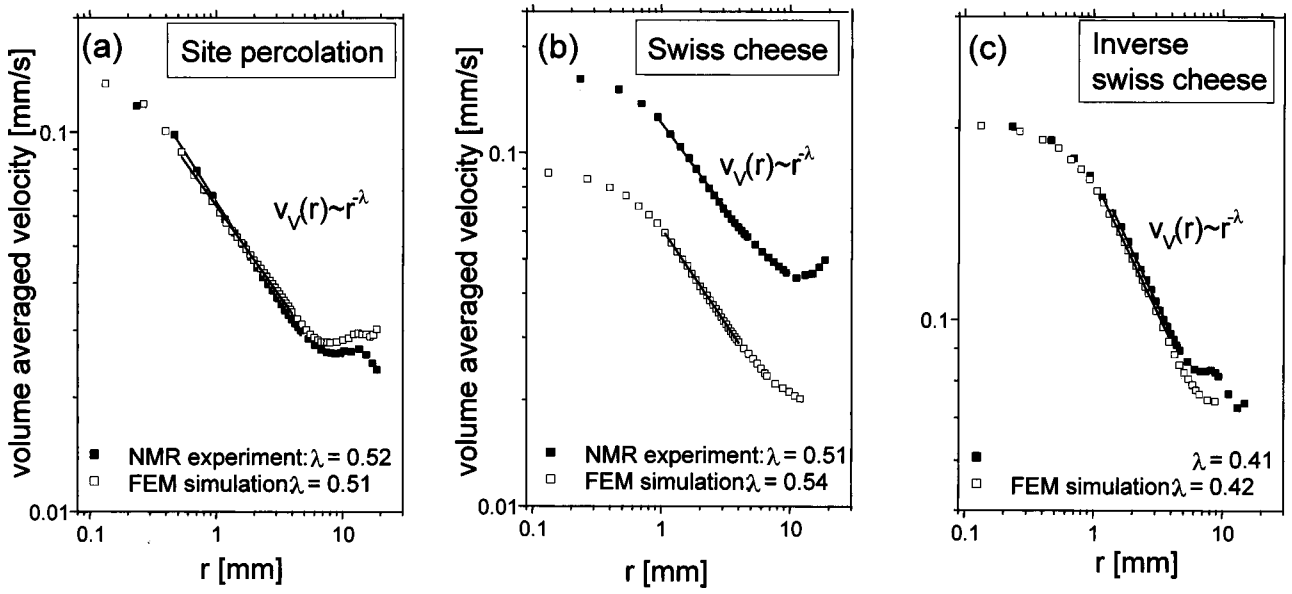

FIG. 9. Volume-averaged velocity as a function of the probe volume radius. The data have been evaluated from the experimental and FEM-simulated velocity maps (see Fig. 6) according to Eq. (3). (a) ''Site percolation,'' $p=0.641$, $p-p_c=0.0467$; (b) ''swiss cheese,'' $p=0.482$, $p-p_c=0.113$; (c) ''inverse swiss cheese,'' $p=0.692$, $p-p_c=0.112$.

those where flow resistance is lowest. This is in contrast with the skeleton definitions used in the computer simulations mentioned above. Keeping in mind that our experiments refer to real flow through the percolation clusters, we conclude that the two fractal-dimension values define the upper and lower limits of the range in which real experimental values can be expected. As a matter of fact, the average value $\langle d_{fback}^{exp}\rangle = 1.46$ determined in the present study lies well within the range predicted by computer simulations of the skeleton and the backbone.

In Table I our experimental fractal-dimension data are compared with those derived from our FEM simulations using the same velocity-related criterion as in the evaluation of the experimental data. The fractal dimension of the total pore space is perfectly reproduced in the simulations for all three models. The fractal dimension of the backbone turns out to be reduced again. Taking the average over all three models and all mean porosities leads to the empirical relation

$$\langle d_{fback}^{FEM}\rangle = \langle d_f^{FEM}\rangle - (0.4 \pm 0.1) \tag{6}$$

with error limits defined as before. The average fractal dimension of the simulated backbones of all three models and for all mean porosities is $\langle d_{fback}^{FEM}\rangle = 1.41$.

The volume-averaged velocity (on the backbone) was evaluated from the experimental [Fig. 6(c)] and FEM simulation [Fig. 6(b)] data according to Eq. (3) as a function of the probe volume radius. In analogy with the analysis of the NMR data, the backbone of the simulated percolation clusters was defined by blackening all voxels with velocities $v \leqslant v_{co}$, where the cutoff value v_{co} corresponds to the rms noise value v_n in the experiments. The actual value of v_{co} was adapted to the experimental situation using $(v_{co}/v_{max})_{FEM} = (v_n/v_{max})_{exp}$. The volume-averaged velocity data determined in this way are plotted in Fig. 9. It turned out that the power law

$$\overline{v}_V(r) \propto r^{-\lambda}, \tag{7}$$

is valid for a wide range. The exponent λ is more or less insensitive to the type of the percolation cluster as well as the occupation probability (see Fig. 10). This suggests a universal character of the power law, Eq. (7), and of the value range of the exponents.

IV. DISCUSSION

Flow through random site percolation, swiss cheese, and inverse swiss cheese clusters has been studied by NMR velocity mapping experiments as well as by FEM/FVM simu-

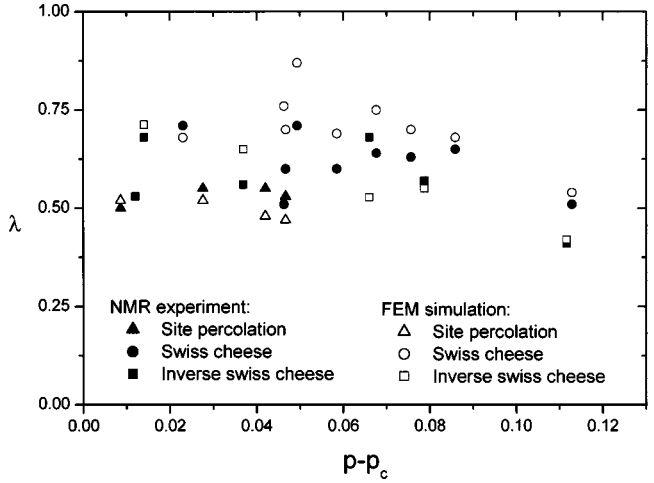

FIG. 10. Exponent λ of the scaling law for the volume-averaged velocity as a function of the occupation probability of the three percolation models.

lations. Monte Carlo generated clusters were used as templates for the fabrication of (quasi-)two- and three-dimensional model objects. The pore space of the sample-spanning cluster was filled with water and rendered in the form of spin density maps. An external pressure gradient was exerted and velocity maps were recorded within the clusters. On this basis, the percolation backbones were evaluated.

The perfect coincidence of the experimental spin density and velocity maps with the Monte Carlo generated templates and FEM/FVM-simulated flow patterns, respectively, prove that the fabrication process, the measuring technique, and the evaluation procedure can be considered to be reliable procedures. One of the conclusions is that parameters such as the fractal dimension, the correlation length, and the percolation probability both of the total clusters and the percolation backbones can safely be determined with computer simulation techniques. The same applies to the volume-averaged velocity that was found to scale with the probe volume radius for a wide range in the form of a power law. The exponent of this law depends only weakly on the porosity and the type of the percolation models considered in this study. A theoretical linkage to the fractal dimension evaluated from the volume-averaged porosity appears to be plausible, but has not yet been established.

While the present study solely refers to the three simplest percolation models, natural systems such as sponge, pumice, sand beds, etc. have been examined in our previous work [12]. The comparison suggests that the pore spaces in the models considered here are too weakly cross linked to be able to represent natural systems. This, in particular, reveals itself by the big difference in the fractal dimensions of the total cluster and the backbones. The natural samples considered so far tend to coinciding values for both fractal dimensions. The conclusion is that correlated (or Ising) site percolation models [20,21] should be more adequate for real porous materials. A corresponding study is in preparation.

ACKNOWLEDGMENTS

This work was supported by the Deutsche Forschungsgemeinschaft.

[1] M. Sahimi, *Flow and Transport in Porous Media and Fractured Rock* (VCH, Weinheim, 1995).
[2] *Methods in the Physics of Porous Media*, edited by P.-Z. Wong (Academic Press, San Diego, 1999).
[3] *Handbook of Porous Media*, edited by K. Vafai (Dekker, New York, 2000).
[4] H. Hermann, *Stochastic Models of Heterogeneous Materials* (Trans Tech Zurich, 1991).
[5] P. M. Adler and J.-F. Thovert, Appl. Mech. Rev. **51**, 537 (1998).
[6] D. Stauffer and A. Aharony, *Introduction to Percolation Theory* (Taylor & Francis, London, 1992).
[7] *Fractals and Disordered Systems* edited by A. Bunde and S. Havlin (Springer-Verlag, Berlin, 1996).
[8] S. Feng, B. I. Halperin, and P. N. Sen, Phys. Rev. B **35**, 197 (1987).
[9] P. M. Adler, C. G. Jacquin, and J. A. Quiblier, Int. J. Multiphase Flow **16**, 691 (1990).
[10] H.-P. Müller, J. Weis, and R. Kimmich, Phys. Rev. E **52**, 5195 (1995).
[11] H.-P. Müller, R. Kimmich, and J. Weis, Phys. Rev. E **54**, 5278 (1996).
[12] A. Klemm, H.-P. Müller, and R. Kimmich, Phys. Rev. E **55**, 4413 (1997).
[13] R. Kimmich, *NMR Tomography, Diffusometry, Relaxometry* (Springer-Verlag, Berlin, 1997).
[14] N. Jan, Physica A **266**, 72 (1999).
[15] J. Mastorakos and P. Argyrakis, Phys. Rev. E **48**, 4847 (1993).
[16] J. S. Andrade, Jr., M. P. Almeida, J. Mendes Filho, S. Havlin, B. Suki, and H. E. Stanley, Phys. Rev. Lett. **79**, 3901 (1997).
[17] A. Kapitulnik, A. Aharony, G. Deutscher, and D. Stauffer, J. Phys. A **16**, L269 (1983).
[18] H. J. Herrmann, D. C. Hong, and H. E. Stanley, J. Phys. A **17**, L261 (1984).
[19] M. Porto, A. Bunde, S. Havlin, and H. E. Roman, Phys. Rev. E **56**, 1667 (1997).
[20] J. Chalupa, P. L. Leath, and G. R. Reich, J. Phys. C **12**, L31 (1981).
[21] J. Adler and A. Aharony, J. Phys. A **21**, 1387 (1988).